Chinese Journal of Aeronautics, (2018), 31(12): 2221–2233

Chinese Society of Aeronautics and Astronautics
& Beihang University

Chinese Journal of Aeronautics

cja@buaa.edu.cn
www.sciencedirect.com

Investigation of straightforward impedance eduction method on single-degree-of-freedom acoustic liners

Xianghai QIU, Bo XIN, Long WU, Yang MENG, Xiaodong JING *

Fluid and Acoustic Engineering Laboratory, School of Energy and Power Engineering, Beihang University, Beijing 100083, China

Received 29 September 2017; revised 9 March 2018; accepted 17 May 2018
Available online 5 September 2018

KEYWORDS

Acoustic liner;
Experimental validation;
Grazing flow effect;
High sound intensity effect;
Impedance eduction;
Numerical evaluation;
Straightforward impedance eduction method

Abstract In order to address the current aircraft noise problem, the knowledge of impedance of acoustic liners subjected to high-intensity sound and grazing flow is of crucial importance to the design of high-efficiency acoustic nacelles. To this end, the present study is twofold. Firstly, the StraightForward impedance eduction Method (SFM) is evaluated by the strategy that the impedance of a liner specimen is firstly experimentally educed on a flow duct using the SFM, and then its accuracy is checked by comparing the numerical prediction with the measured wall sound pressure of the flow duct. Secondly, the effects of grazing flow and high-intensity sound on the impedance behavior of two single-layer liners are investigated based on comparisons between educed impedance and predictions by three impedance models. The performance of the SFM is validated by showing that the educed impedance leads to excellent agreement between the simulation and the measured wall sound pressure for different grazing flow Mach numbers and Sound Pressure Levels (SPLs) and over a frequency range from 3000 Hz down to 500 Hz. The grazing flow effect generally has the tendency that the acoustic resistance exhibits a slight decrease before it increases linearly with an increase in Mach, predicted successfully by the sound-vortex interaction theoretical model and the Kooi semi-empirical impedance model. However, the Goodrich semi-empirical impedance model gives only a simple linear relation of acoustic resistance starting from Mach zero. Additionally, when the SPL increases from 110 to 140 dB in the present investigation, the acoustic resistance exhibits a significant increase at all frequencies in the absence of flow; however, the resistance decreases slightly under a grazing flow of Mach 0.117. It indicates that the SPL effect can be greatly inhibited when flow is present, and the grazing flow effect can be reduced partly as well at a relatively high SPL.

* Corresponding author.
E-mail address: jingxd@buaa.edu.cn (X. JING).
Peer review under responsibility of Editorial Committee of CJA.

Production and hosting by Elsevier

https://doi.org/10.1016/j.cja.2018.08.014

1. Introduction

For modern turbofan engines with high bypass ratios, fan noise is the main contributor of noise radiation. However, it becomes increasingly more difficult to reduce the fan noise by using acoustic liners in the inlet and outlet ducts of the nacelles as the bypass ratio increases. The noise-absorbing efficiency of the acoustic liners is expected to be enhanced to a level higher than ever before, for which the knowledge of impedance of the acoustic liners subjected to high-intensity sound and grazing flow is of crucial importance to both the optimization of liner parameters[1] and the development of new liner concepts.

For a locally reacting acoustic liner, its impedance can be educed on a flow duct in which the grazing flow and high Sound Pressure Level (SPL) conditions, typically encountered in acoustic nacelles, can be experimentally simulated. Both iterative[2–5] and StraightForward impedance eduction Methods (SFMs)[6,7] have been developed and continually improved[8,9] to obtain the impedance of a liner specimen from the information of the wall sound pressure measured on the flow duct. Iterative methods (also known as objective function methods) search the unknown impedance iteratively from minimizing the objective function given by the residual error between measured and computed wall sound pressures of the flow duct. Therefore, forward computation is necessary to predict the wall sound pressure for their implementation, for which various duct propagation models have been set up and employed, such as finite element models solving convective Helmholtz equations[10] or linearized Euler equations.[11] The iteration begins from an initial guess and proceeds until the objective function is satisfactorily small, but a convergence problem may occur on some occasions.[12] The straightforward method, on the other hand, can realize the impedance eduction with a simple, direct computation. The basic idea of the SFM is decomposing the measured distribution of the wall sound pressure into a series of acoustic modes by means of Prony's method[13,14] or its variants such as the Kumaresan and Tufts (KT) algorithm.[15] With the information of the complex axial wave number of the dominant or least-attenuated mode, the SFM calculates the unknown impedance directly from the eigen-equation. Since the SFM only solves the eigen-equation instead of the complete boundary value problem for duct sound propagation, the method can be implemented without knowing the boundary conditions on the source and exit planes. This is a benefit since the measurement errors in the two boundary conditions may result in some abnormal discrepancy in impedance eduction results, as reported for iterative methods.[16] As a direct method without the need for iteration, the SFM has no convergence problem and promises a higher computational efficiency. Recently, there has been an increasing interest in doing comparative investigations of the two different impedance eduction methods.[15,17] According to Watson et al.[15] the efficiency of the straightforward method can be one to two orders higher than those of iterative methods. As for the accuracy, it has been shown that there is generally good agreement between the two methods except at the extremely low-frequency end and near the anti-resonant points.

Note that there is no research on the accuracy of the educed impedance by the SFM in terms of sound propagation prediction using the educed impedance. It is fairly necessary to conduct this kind of research, since the purpose of impedance eduction is to predict sound attenuation in the design of an aircraft acoustic nacelle. In this study, such an accuracy evaluation of the SFM is firstly carried out. The evaluation begins with experimental eduction of the impedance of two Single-Degree-Of-Freedom (SDOF) liner specimens on a flow duct using the SFM, then the educed impedance along with the measured acoustic information on the source and exit planes is employed in FEM simulation to solve the sound field, and the impedance accuracy is finally checked by comparing the numerical simulation with the measured wall sound pressure of the flow duct, which is feasible since the SFM, unlike an iterative method,[10,18] does not involve numerical computation solving a complete boundary value problem of a duct propagation model. Secondly, the effects of the grazing flow and high sound intensity on the impedance behavior of the SDOF liners are investigated. For a quantitative study of the grazing flow acoustic resistance, predictions by three impedance models[19–21] are compared with the impedance eduction results of the SFM. The KooI semi-empirical model (KI) presents generally good agreements with experimental data. The Sound-Vortex interaction model based on the Particle Velocity Match (PVM-SV) also reproduces the sinking region and the linearly increasing region. However, the GoodRich semi-empirical model (GR) fails to predict the sinking region, and instead, gives only the simple linear relation of resistance starting from zero flow speed. In addition, the educed impedance when the SPL on the source plane increases from 110 dB up to 140 dB in the presence or absence of grazing flow is compared and analyzed. It is indicated that the SPL effect can be greatly inhibited when grazing flow is present, and the grazing flow effect can be reduced partly as well at a relatively high SPL.

2. Problem description and methods: Impedance eduction and duct propagation

2.1. Straightforward impedance eduction

As depicted in Fig. 1 an acoustic liner of a finite length L, whose acoustic impedance is Z is placed on the lower wall of a rectangular duct with height b. There is uniform flow passing the liner from left to right in the duct. Plane sound wave generated in the upstream hardwall section of the duct is grazingly incident upon the acoustic liner. A coordinate system is introduced with the x and y axes being along the axial and vertical directions, respectively, whose origin is defined on the upper duct wall over the leading edge of the liner. The problem of impedance eduction is how to precisely and efficiently deduce the unknown impedance Z from the information of the acoustic pressure acquired on the flow duct wall. For this purpose, J equally-spaced microphones mounted on the upper wall opposite to the liner are used to measure the acoustic pressure. The microphones J_i^S and J_i^E ($i = 1, 2$) are used to measure the acoustic pressures near the source and exit planes, respectively.

The sound field in the flow duct is governed by the convective Helmholtz equation, as below:

$$\left(\mathrm{i}k + Ma\frac{\partial}{\partial x}\right)^2\phi - \nabla^2\phi = 0 \tag{1}$$

where $\mathrm{i} = \sqrt{-1}$, $k = \omega/c_0$ is the free space wavenumber, with ω being the angular frequency and c_0 being the speed of sound;

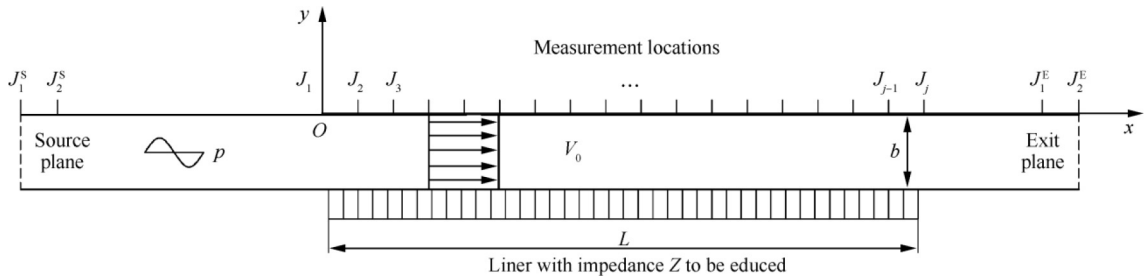

Fig. 1 Illustration of flow duct of SFM.

$Ma = V_0/c_0$, is the Mach number with V_0 being the flow velocity; the acoustic velocity potential ϕ is related to the acoustic pressure as

$$p = -\rho_0 c_0 \left(\mathrm{i}k + Ma\frac{\partial}{\partial x}\right)\phi \tag{2}$$

where ρ_0 is the mean density of air. The wall impedance boundary condition for a locally reacting liner can be described as follows [22,23]:

$$\frac{\partial p}{\partial y} = \left(\mathrm{i}k + 2Ma\frac{\partial}{\partial x} + \frac{Ma^2}{\mathrm{i}k}\cdot\frac{\partial^2}{\partial x^2}\right)\frac{p}{Z} \tag{3}$$

Owing to the uniformity of the boundary conditions in the z direction, the sound field can be regarded as a two-dimensional problem with no dependence of the z coordinate in the flow duct. The sound pressure related with the acoustic velocity potential can be decomposed into modal contents as

$$p = \sum_{n=1}^{\infty} A_n^+ \cos\left(k_{yn}^+ y\right)\mathrm{e}^{-\mathrm{i}k_{xn}^+ x} + A_n^- \cos\left(k_{yn}^- y\right)\mathrm{e}^{-\mathrm{i}k_{xn}^- x} \tag{4}$$

where $A_n^\pm$ and $k_{xn}^\pm$ are the complex modal amplitudes and axial complex wavenumbers of the n-th decomposed mode, respectively, with superscript $\pm$ representing forward and backward modes, respectively. The dispersion relation is described as follows:

$$k_{xn}^\pm = \frac{-Mak \pm \sqrt{k^2 - (1-Ma^2)\left(k_{yn}^\pm\right)^2}}{1-Ma^2} \tag{5}$$

which relates the axial wavenumbers with the vertical wavenumbers, $k_{yn}^\pm$. In the lined section, the impedance boundary condition, Eq. (3), leads to the following y direction eigenequation:

$$Z = \frac{\mathrm{i}k}{k_{yn}^\pm \tan\left(k_{yn}^\pm b\right)}\left[\frac{1}{1-Ma^2}\left(1 \mp Ma\sqrt{1-\frac{1-Ma^2}{k^2}\left(k_{yn}^\pm\right)^2}\right)\right]^2 \tag{6}$$

In practice, Eq. (4) is truncated up to the N-th order modes. Substituting the acoustic pressure measured on the J locations of the upper wall where $y = 0$, a set of nonlinear equations is obtained as

$$p_j^{\mathrm{U}} = \sum_{n=1}^{N} A_n \mathrm{e}^{-\mathrm{i}k_{xn}j\Delta x} \qquad j = 1, 2, \ldots, J \tag{7}$$

where superscript U represents the upper wall, Δx is the spacing between two adjacent microphones, and J must be not less than $2N$. Note that Eq. (7) includes both forward and backward acoustic modes, and superscript $\pm$ has been omitted.

In the straightforward impedance eduction method, Prony's method is employed to transform Eq. (7) into a linear least-squared problem, by solving which the axial complex wavenumbers k_{xn} and the corresponding amplitudes A_n are educed from the sampled upper wall sound pressure. Then, the unknown impedance of the acoustic liner is simply calculated from the Eq. (6), where the vertical complex wavenumbers, k_{yn}, is calculated from the dispersion relation, Eq. (5).

2.2. Duct propagation

The boundary conditions on the source and exit planes are not considered in the formulation of the straightforward impedance eduction method. Therefore, unlike NASA's objective function method, the straightforward method does not depend on computing the whole sound field in the flow duct. Therefore, by the strategy of investigating whether the educed impedance can numerically reproduce the measured sound field, the duct propagation problem is fairly suitable for the assessment of the educed accuracy of the SFM. In the problem of duct propagation, the whole sound field can be solved from the boundary value problem formed by imposing the impedance boundary condition on the liner surface, the impervious boundary condition on the hard walls, as well as the boundary conditions on the source and the exit planes using the convective Helmholtz Eq. (1).

The velocity potential boundary conditions on the source and exit planes can be determined from the acoustic pressure measured by the two pairs of microphones deployed near the source and exit planes, respectively, as shown in Fig. 1. Below the cutoff frequency of higher-order modes, only plane wave can propagate in the hardwall section away from the discontinuities between the hardwall and the liner, so the sound field consists of incident and reflected plane modes as follows:

$$p = A^+\mathrm{e}^{-\mathrm{i}k^+x} + A^-\mathrm{e}^{-\mathrm{i}k^-x}$$

where $A^\pm$ and $k^\pm = k/(Ma \pm 1)$ are the complex amplitudes and axial wavenumbers of the forward and backward modes, respectively. Therefore, near the source plane, the acoustic pressure p_i $(i = 1, 2)$ measured by Microphones J_1^S and J_2^S at the two locations x_i can be written as

$$p_i = A^+\mathrm{e}^{-\mathrm{i}k^+x_i} + A^-\mathrm{e}^{-\mathrm{i}k^-x_i} \tag{8}$$

From the two linear equations above, the complex amplitudes $A^\pm$ can be solved for the forward and backward propagating waves, respectively. This is actually the principle of the

two-microphone method.[24–26] Then, according to Eq. (2), the velocity potential on the source plane is calculated as below:

$$\phi_S = \phi_S^+ + \phi_S^- = \frac{A^+ e^{-ik^+ x_1}}{-i\rho_0(\omega - V_0 k^+)} + \frac{A^- e^{-ik^- x_1}}{-i\rho_0(\omega - V_0 k^-)} \quad (9)$$

The velocity potential ϕ_E on the exit plane can be determined similarly. The governing Eq. (1), combined with the inlet and outlet boundary conditions and the impedance boundary condition, can fully describe the sound propagation problem.

A finite element method is used to solve the boundary value problem. The strategy is that the product of the governing Eq. (1) and weighting functions is integrated over the computational domain, then the integration can be discretized using a discontinuous Galerkin formulation, a set of linear equations can be obtained by substituting the boundary conditions into the discontinuous Galerkin formulation, and finally the sound field in the duct can be solved from the linear equations.

3. Experiment

Fig. 2 shows a schematic of the flow duct test rig in the Fluid and Acoustic Engineering Laboratory (FAEL) at BUAA. The flow is provided by a continuous wind tunnel consisting of a centrifugal fan, plenum with metal screens, and silencing ducts.

The flow duct has a 51 mm × 51 mm square cross section. The test liner is flush installed with its facing sheet forming a portion of the lower wall of the flow duct. The sound source consists of four BMS 4592 loudspeakers. The driven signal of the loudspeakers is fed by an NI USB-6259 AO channel connected to a power amplifier. There are totally 22 flush-mounted 1/4 inch (1 inch = 25.4 mm) microphones of GRAS type 40BH on the upper duct wall, 16 of which being positioned right above the test liner to measure the sound pressure profile due to the attenuation of the liner. The microphone at the liner entrance is also used to provide the phase reference and to monitor the SPL there. One pair of microphones with a spacing of 25 mm are located upstream with the nearer one being 180 mm away from the microphone at the liner entrance, which are used to measure the boundary condition on the source plane; another pair of microphones are located in the downstream position 80 mm away from the microphone at the liner exit. All the microphones are calibrated in a plane wave tube to minimize their phase and amplitude mismatch. The acquisitions of microphone signals are conducted through an NI PXI-4496 multichannel AI device. Acoustic amplitude and phase of each channel are achieved by a cross-spectrum analysis between that channel and the channel of the reference microphone at the liner entrance. A two-dimensional flow profile is measured by a traversing pitot tube at 16 by 9 grid points over the cross-section of the duct, which is used to calculate the average velocity. In addition, the wall temperature inside the flow duct is measured by a flush-mounted TP3001 thermometer, and the ambient pressure by a mercury barometer.

Two pieces of aluminum perforated liners are tested, whose overall size is 400 mm in length and 51 mm in width. The perforated liners are the type of single degree of freedom that consists of a perforated facing sheet backed by one layer of resonant cavity. The cavities of the liners are made of honeycomb structures, ensuring the liners' locally reacting characteristics. The geometrical parameters of the liners including the orifice diameter d, plate thickness t, porosity σ, and cavity depth L_c are given in Table 1.

An experiment is carried out at 7 grazing flow Mach numbers, which are 0, 0.029, 0.059, 0.087, 0.117, 0.146, 0.175, and 0.220, and four SPL_{SP} of 110, 120, 130, and 140 dB as the tonal frequency varies from 500 to 3000 Hz in steps of 500 Hz, where subscript SP indicates that the SPLs are those measured on the source plane. Note that the grazing flow Mach numbers are calculated from averaging the two-dimensional flow profile measured over the cross section of the duct, which correspond to centerline flow speeds of 0, 0.037, 0.076, 0.112, 0.151, 0.188, 0.226, and 0.284, respectively.

4. Validation of impedance eduction

4.1. Hardwall verification

A piece of 20 mm-thick aluminum block is used as the hard-wall specimen. In accordance with the boundary condition of

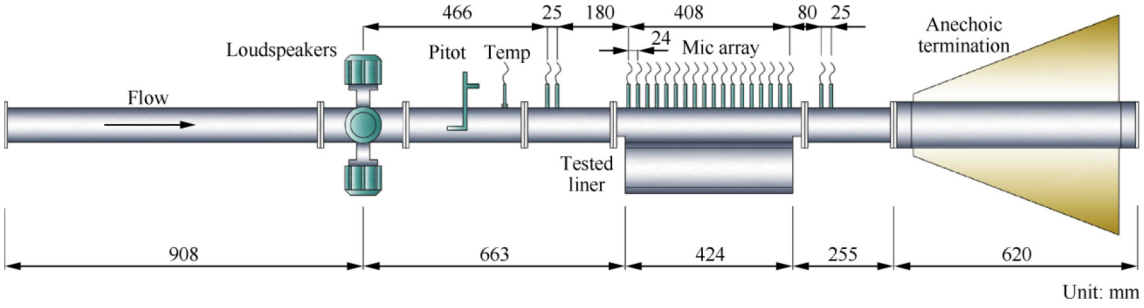

Fig. 2 Schematic of grazing flow duct.

Table 1 Geometrical parameters of tested liners.

Liner No.	Hole diameter d (mm)	Perforated plate thickness t (mm)	Porosity σ (%)	Cavity depth L_c (mm)
1	1.0	1.0	6.81	23.0
2	1.0	0.8	8.35	38.0

vanishing normal particle velocity, the expected value of the admittance, which is the inverse of acoustic impedance, is zero for a hardwall specimen. Fig. 3 shows the normalized admittance of the hardwall specimen educed by the SFM for a no-flow condition and $Ma = 0.220$. Under a no-flow condition, the educed admittance, whose real part (conductance) and imaginary part (susceptance) are less than 0.05, is in excellent agreement with the expected value of zero. When the Mach number increases to 0.220, it is seen that the educed conductance remains unaffected, whereas the magnitude of the educed susceptance slightly increases with an increase in the frequency. The slight deviation of the educed susceptance from the expected value of zero may be due to the existence of a boundary layer and its interaction with the sound wave. Generally speaking, the SFM obtains the excepted admittance of the hardwall with a good accuracy.

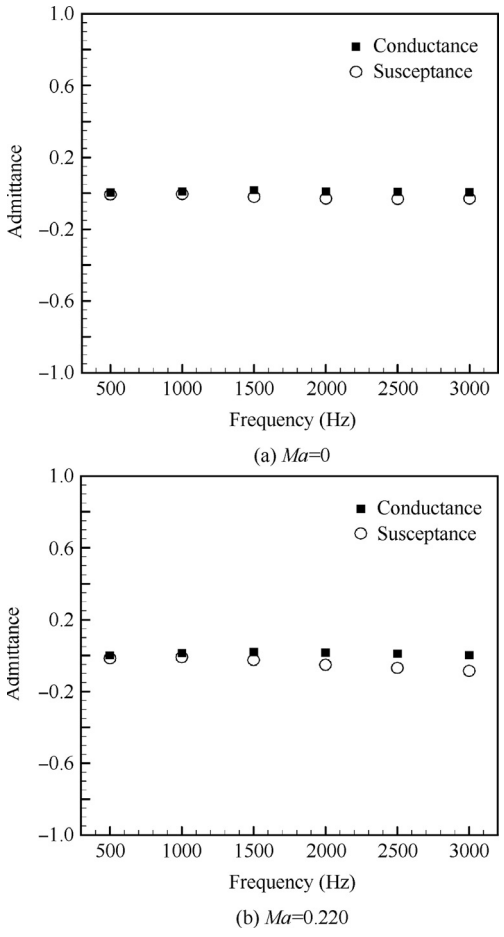

Fig. 3 Educed normalized admittance of hardwall insert at $SPL_{SP} = 130$ dB.

4.2. Comparison between predicted and measured wall sound pressures

As mentioned before, the SFM does not need to compute the whole sound pressure field in the flow duct, and it even does not depend on the boundary conditions on the source and exit planes. Therefore, the main purpose of this section is to see how well the prediction of a duct propagation model, which is based on the educed impedance by the SFM imposed on the soft boundary, agrees with the sound pressure measured on the duct wall. Eventually, from the point of view of application, the accuracy of a method for impedance eduction or measurement should be assessed by the fact whether the educed or measured impedance can result in a better prediction of acoustic attenuation.

Fig. 4 shows the computational domain and numerical probe locations of the duct propagation model. The resolution of the computational mesh ensures at least 15 points-per-wavelength, and the mesh is further refined at the entrance and exit of the liner where there are discontinuities of wall boundary condition. The impedance Boundary Condition (BC) is imposed by the educed impedance by the SFM. The inlet and outlet boundary conditions are calculated from the measured acoustic pressure by the two microphone pairs, respectively, as described in Section 2.2. A finite element simulation of the sound field is carried out by means of the commercial software COMSOL.

Figs. 5–8 show comparisons of acoustic pressures along the upper wall opposite to the liner. Here, only results pertaining to liner No. 1 are presented. All the educed impedances of liner No. 1 are provided in the matrix of Table 2 at different frequencies and Mach numbers. Watson et al.[16] suggested using the acoustic pressure boundary condition on the exit plane instead of the impedance boundary condition in the FEM simulation because the error in the latter may cause unexpected discrepancies of results. In the present introduction, the sound fields can be decomposed into forward and backward plane modes in the hardwall sections by means of the two-microphone method, which are used to calculate the acoustic potential by Eq. (9) to provide the boundary conditions on the source and exit planes. The acoustic pressure amplitudes A_m and phases P_h measured by the two-microphone pairs at $SPL_{SP} = 130$ dB for liner No.1 are presented in Table A1 of

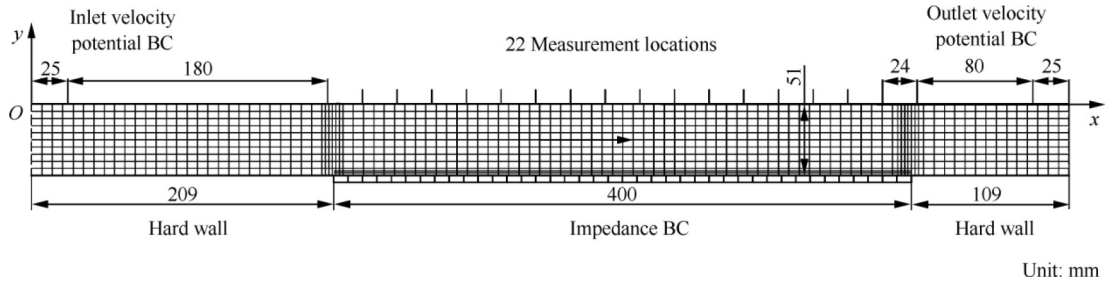

Fig. 4 Illustration of computational model.

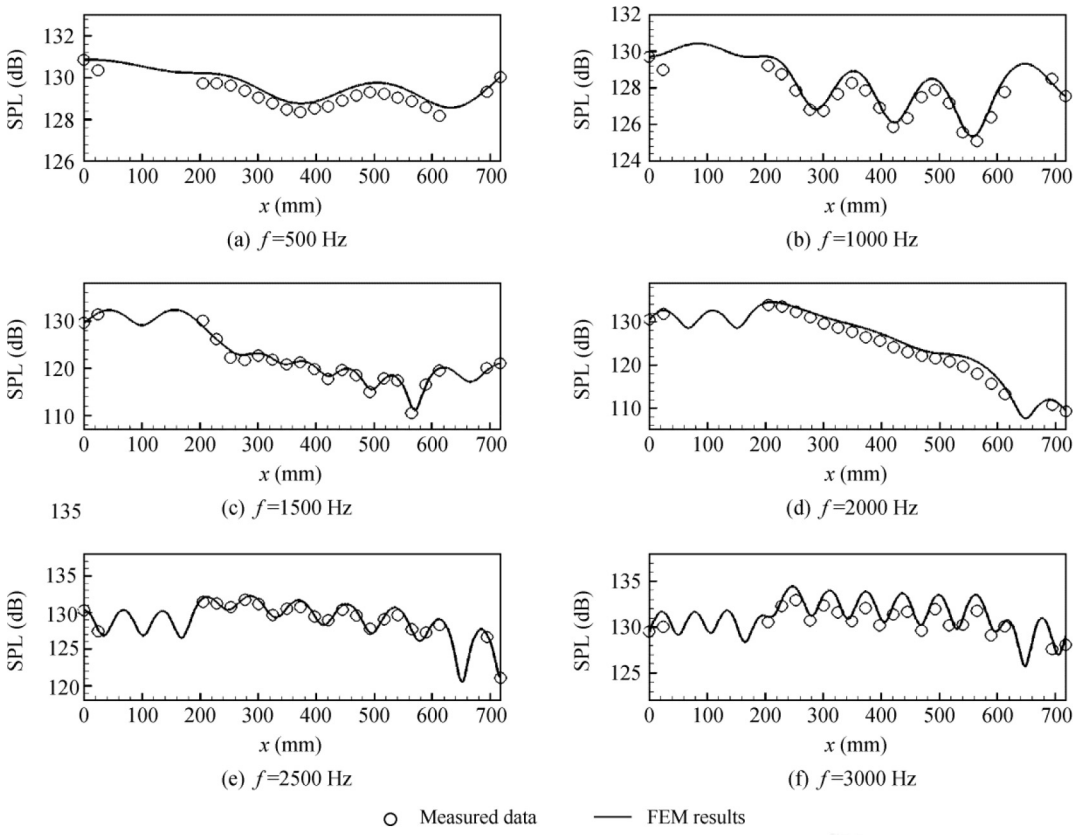

Fig. 5 Comparisons of SPL between measured data and FEM results for liner No. 1 at SPL_{SP} = 130 dB and Ma = 0.

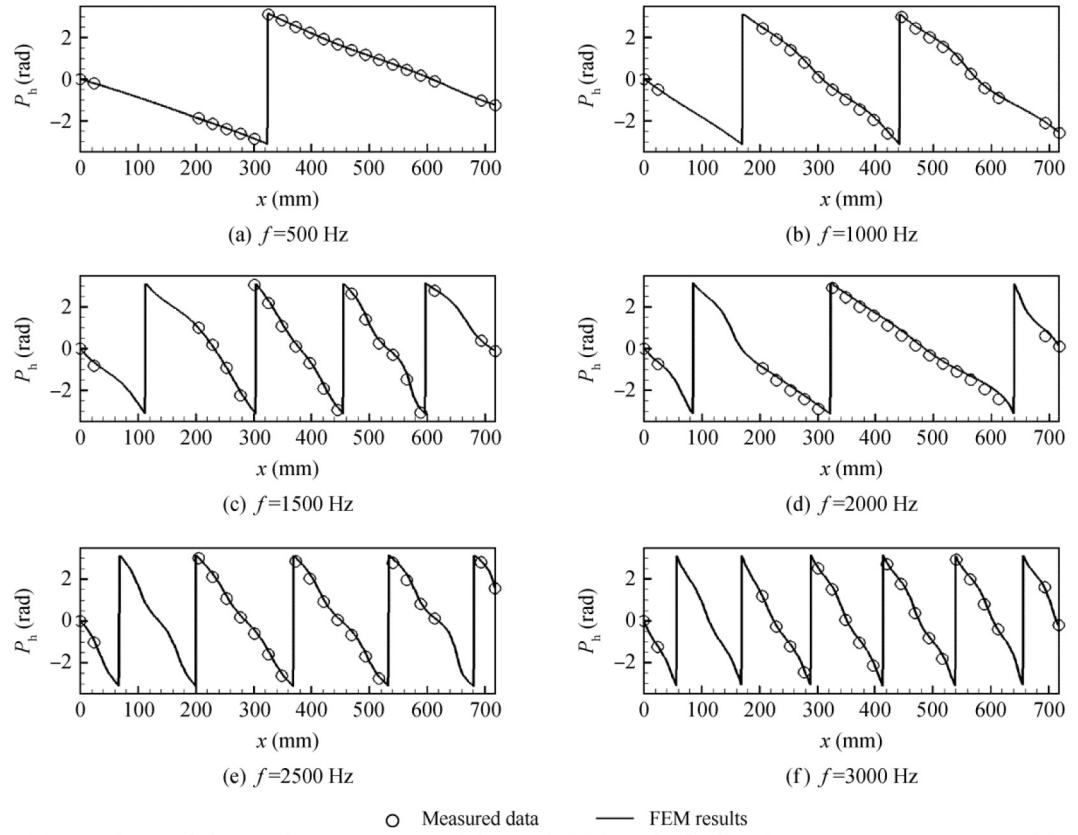

Fig. 6 Comparisons of P_h between measured data and FEM results for liner No. 1 at SPL_{SP} = 130 dB and Ma = 0.

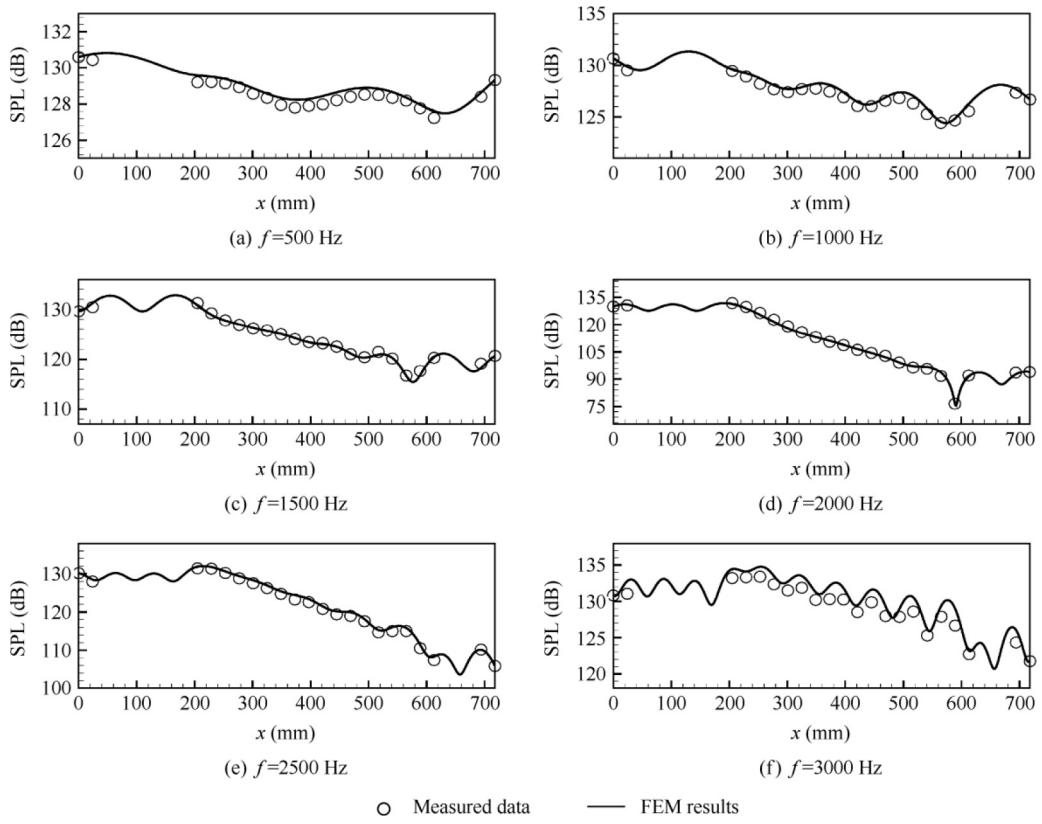

Fig. 7 Comparisons of SPL between measured data and FEM results for liner No. 1 at SPL_{SP} = 130 dB and Ma = 0.146.

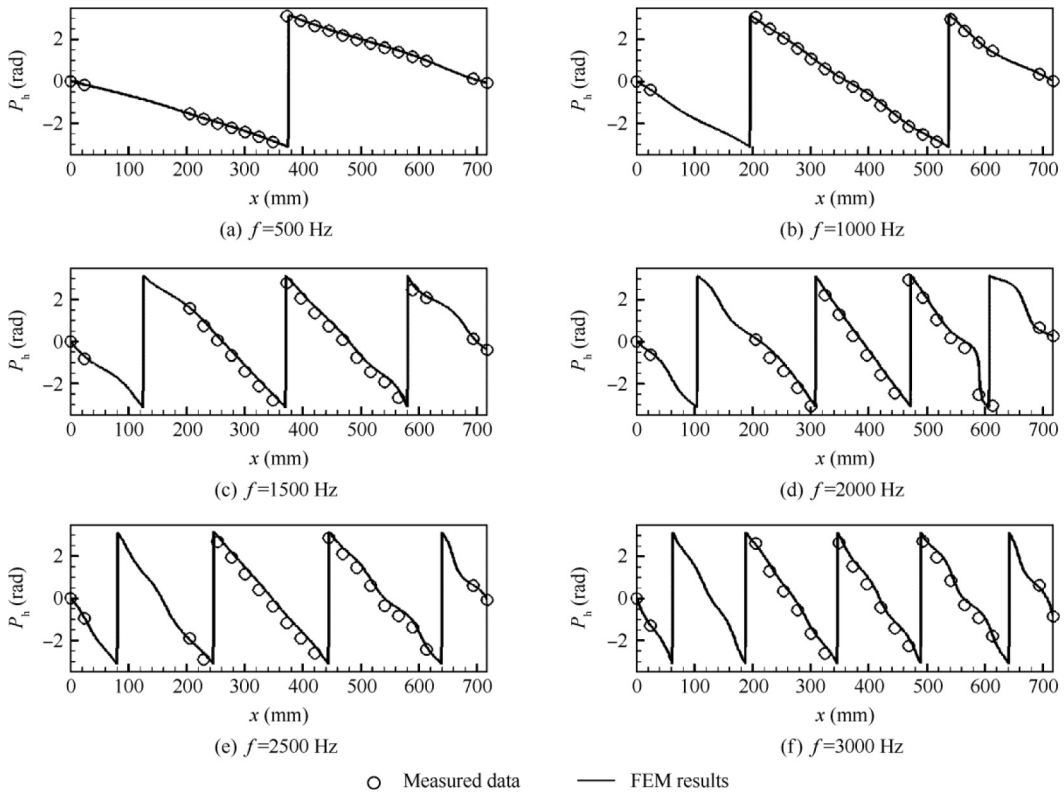

Fig. 8 Comparisons of P_h between measured data and FEM results for liner No. 1 at SPL_{SP} = 130 dB and Ma = 0.146.

Table 2 Impedances educed by SFM at SPL_{SP} = 130 dB for liner No. 1.

Ma	*T* (K)	500 Hz		1000 Hz		1500 Hz		2000 Hz		2500 Hz		3000 Hz	
		Re*Z*	Im*Z*	Re*Z*	Im*Z*	Re*Z*	Im*Z*	Re*Z*	Im*Z*	Re*Z*	Im*Z*	Re*Z*	Im*Z*
0	285.60	0.540	−4.993	0.201	−2.113	0.166	−0.954	0.162	−0.105	0.156	0.360	0.152	0.800
0.029	286.05	0.588	−4.995	0.198	−2.124	0.150	−0.942	0.159	−0.112	0.140	0.355	0.140	0.785
0.059	286.55	0.808	−4.893	0.324	−2.162	0.197	−1.031	0.160	−0.198	0.107	0.289	0.111	0.727
0.087	287.20	0.930	−4.851	0.518	−2.192	0.374	−1.110	0.318	−0.285	0.215	0.129	0.158	0.549
0.117	287.85	1.082	−4.825	0.672	−2.182	0.542	−1.120	0.442	−0.293	0.381	0.060	0.317	0.449
0.146	290.95	1.404	−5.138	0.871	−2.307	0.758	−1.181	0.608	−0.531	0.511	0.005	0.444	0.363
0.175	293.20	1.662	−4.884	1.229	−2.442	0.867	−1.179	0.712	−0.543	0.627	−0.022	0.574	0.355
0.220	293.60	2.547	−4.469	1.365	−2.212	1.187	−1.219	0.963	−0.580	0.826	−0.099	0.721	0.270

Appendix A. Figs. 5 and 6 show the magnitudes and phases of the acoustic pressures, respectively, at $Ma = 0$. The subfigures from (a) to (f) correspond to frequencies from 500 to 3000 Hz in steps of 500 Hz, respectively. It can be seen that the FEM simulations, which are obtained using the impedances (first column of Table 2) educed by the SFM, are in fairly good agreement with the measured acoustic pressure along the duct wall. This indicates that the impedance of the liner is educed with a very good accuracy. The validation is demonstrated for both the cases of near resonance where the liner produces large attenuation and the cases of near anti-resonance where the liner becomes less absorptive. Results at $Ma = 0.146$ are shown in Figs. 7 and 8 for the magnitudes and phases, respectively, which exhibit better agreement between the FEM simulations and the acoustic measurements than the observations at $Ma = 0$.

According to previous investigations,[27,28] if there occurs a longitudinal resonance inside the flow duct, it can cause larger uncertainty in the educed impedance; consequently for such a situation, the numerical prediction showed large deviation from the measured acoustic pressure along the duct wall.[29–32] In the present case, it seems that we have not encountered the longitudinal resonance since the FEM predictions show equally good agreement with the measurements for all the frequencies, which are more satisfactory than those similar comparisons.[29–32] Therefore, the educed impedances are accurate enough to afford reliable numerical predictions of acoustic propagation in the lined duct in the absence or presence of grazing flow and at frequencies from 3000 Hz to a frequency as low as 500 Hz. The validation of the SFM accuracy is conducted by means of comparing the numerical and experimental sound fields for the first time, and such a good accuracy strengthens the confidence in the later analyses on educed results.

5. Investigation into effects of grazing flow and high SPLs

The normalized specific acoustic impedance of a perforated liner of single degree of freedom can be formulated as below:

$$Z = R + \mathrm{i}X = R(t, d, f, Ma, \mathrm{SPL})/\sigma + \mathrm{i}[k(t+\delta)/\sigma - \cot(kL_c)]$$

where R and X are the resistance and reactance, respectively; mass reactance $k(t+\delta)/\sigma$, related to oscillating fluid slug of length $t+\delta$, in which δ is the end correction.

The acoustic impedance of the perforated plate is related to the acoustic resistance and mass reactance of the orifice on the assumption that the interaction between the orifices, if they are sparsely distributed, can be neglected.

Thus, the acoustic impedance is not only a function of geometrical parameters (orifice diameter d, plate thickness t, porosity σ, and cavity depth L_c) and frequency, but also depends on the SPL and grazing flow conditions. Therefore, the knowledge of the so-called "grazing flow effect" is of essential importance to design and optimization of perforated liners.

5.1. Grazing flow effect

Fig. 9 presents the impedance spectra of two liners at different grazing flow Mach numbers: $Ma = 0$, 0.087, 0.146, and 0.220. As clearly revealed by experimental results, the acoustic resistance proportionally increases, while the acoustic reactance drops slightly with an increase in the grazing flow Mach number. There is also a trend that the acoustic resistance decreases with an increase in the frequency for a fixed Mach number. It has been recognized that the grazing flow effect is due to the mechanism of sound vortex interaction. The acoustic motion perturbs the shear layer over the small orifices of perforated liners, causing unsteady vortex shedding at the leading edge of the orifices and thus a conversion of the acoustic energy into the kinetic energy of the shed vortices. In a simple and qualitative way, it can be estimated that the unsteady circulation at the leading edge of an orifice is proportional to the grazing flow Mach number, thus causing an increase in the acoustic resistance. On the other hand, in the vicinity of an orifice, the presence of vortical flow reduces the portion of potential flow that oscillates together with the fluid slug within the orifice, and this "blow-away effect"[21,33,34] of the grazing flow diminishes the mass end correction contributing to the reactance of an orifice. However, how to accurately predict the grazing flow effect is still a challenging problem.

Currently, models for the grazing flow effect generally fall into three categories: semi-empirical models, the sound vortex interaction model,[20] and numerical simulations. Numerical simulation can provide large amounts of detailed physical field information, but the expensive computing cost limits its application in industry design. The sound vortex interaction model is a theoretical model under some appropriate simplifications, good at qualitatively analyzing the grazing flow effect of a perforated plate. Semi-empirical models are widely used in the engineering design process of acoustic liners due to their viability of incorporating various practical influential factors. The

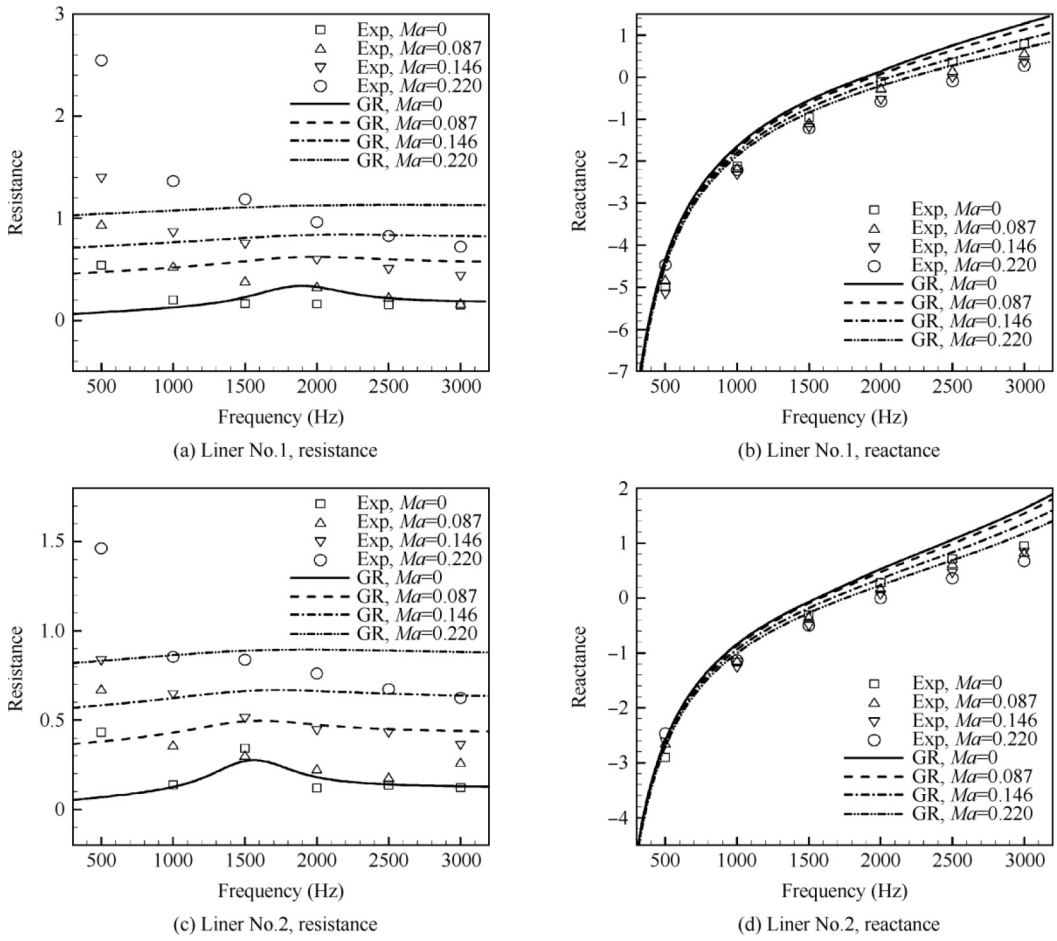

Fig. 9 Comparisons of normalized impedance spectra between experiment and GR model for liners Nos. 1 and 2 at SPL_{SP} = 130 dB with different *Ma*.

development of semi-empirical models is not only based on impedance databases, but also the knowledge of the trends of impedance variation gained by theoretical and numerical models. According to the starting Mach number of the increase of grazing flow acoustic resistance, semi-empirical models can be divided into two types: the starting *Ma* of the first group is zero, for example, the Guess model,[34] the Lewis and Garrison model,[35] and the GR[21]; those of the others are larger than zero, for example, the KI[19] and the Cumming model.[36]

Fig. 10 shows the acoustic resistance of liner No. 1, where the data educed by the SFM is compared with the predictions by GR, KI, and PVM-SV. The former two models represent respectively the two types of semi-empirical impedance models as mentioned above, whereas the later one is a linearized potential flow model in which the effect of a thick shear layer over an orifice, when it interacts with the acoustic motion, is equivalently considered by using the normal particle velocity continuity condition. The experimental data is generally in agreement with the Kooi model and the sound-vortex interaction model in that the acoustic resistance increases very slowly or even drops in the lower range of *Ma*, and then, above a certain value of *Ma*, the acoustic resistance turns to increase linearly with *Ma*. Therefore, this is a more complicated behavior than a linear increase from zero grazing flow Mach number as predicted by the GR.

The demands of accurate prediction of the grazing flow acoustic resistance are twofold. On one hand, the educed resistance grows monotonically in the case of 500 Hz, but drops slightly before it increases with an increasing flow Mach number at higher frequencies, i.e., the upper limit of the grazing flow Mach of the sinking region grows with an increasing frequency. The upper Mach limit is equivalent to the starting *Ma* of the increasing portion, and therefore, must be predicted correctly. The sound-vortex interaction model depicts exactly the details. On the other hand, a proper prediction at high Mach numbers depends directly on the slope of the increasing portion above the starting *Ma*. The KI gives a correct prediction to the second factor; however, the slope predicted by the GR is underestimated at low frequencies, and that by the PVM is overestimated at high frequencies. Through the comparisons above, a potential method is suggested that the prediction of the starting Mach number of the increasing region by the PVM and the empirical correlation of the slope of the linear increase in the KI may be combined together to construct a new model in future research for an accurate prediction of the grazing flow effect.

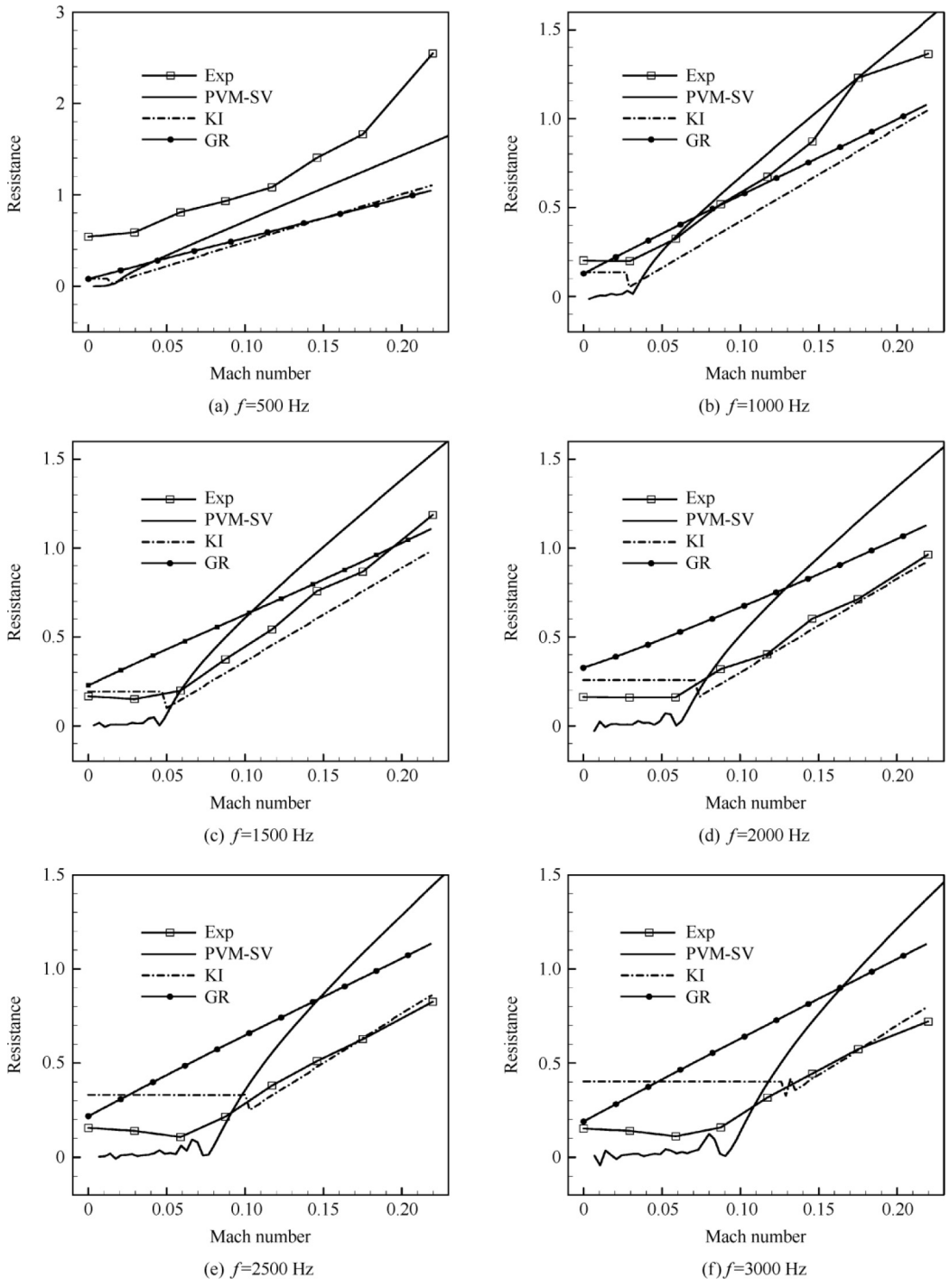

Fig. 10 Normalized resistance varies with grazing flow Mach number for liner No. 1 at an SPL_{SP} = 130 dB with different frequencies.

5.2. Interaction between SPL and grazing flow effects

Firstly, the situation that the SPL_{SP} varies from 110 to 140 dB but there is no grazing flow is considered. For liner No. 2, Figs. 11(a) and (b) shows that an increase in the SPL_{SP} causes little change in the acoustic reactance. On the other hand, the acoustic resistance exhibits a modest increase only at 1500 Hz when the SPL_{SP} increases from 110 to 130 dB, but increases significantly at all frequencies from 500 Hz up to 3000 Hz when the SPL_{SP} reaches 140 dB. The experimental observation is consistent with the physical insights that high-intensity sound can induce vortex shedding from the edge of the orifices of perforated liners, and thus the acoustic resistance increases greatly due to the conversion of the acoustic energy to the kinetic energy of shed vortices. A relevant investigation by means of a direct numerical simulation indicates that the dissipation efficiency of vortex shedding is impressively high, up to 12.5 times as much as that of the viscosity dissipation mecha-

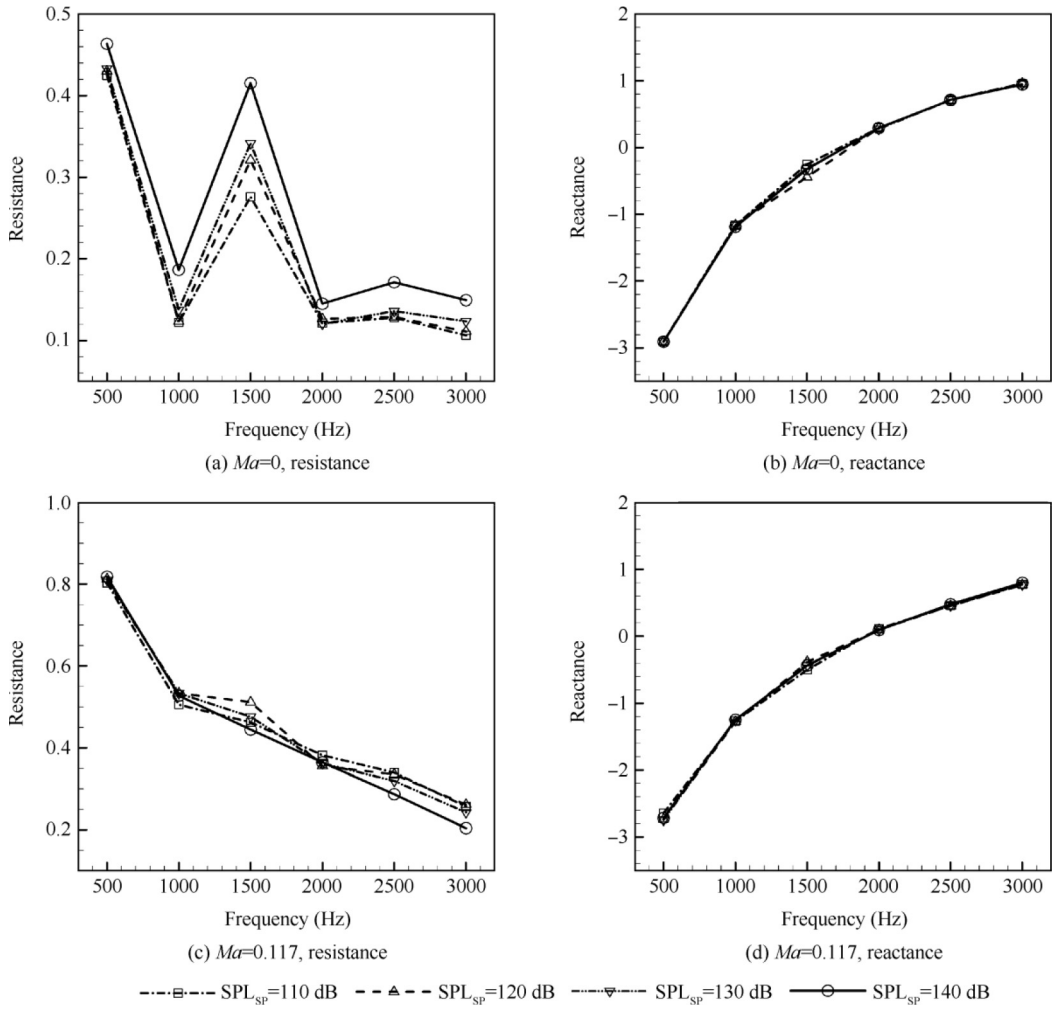

Fig. 11 Comparisons of normalized impedance of liner No. 2 at different SPL_{SP} and *Ma*.

nism in their case.[37] Note that the SPL over a large portion of the tested liner may be considerably lower than the SPL_{SP}, since the acoustic pressure over the liner decreases with distance as a result of sound absorption of the tested liner; therefore, the starting SPL_{SP} of nonlinear effects in a grazing incidence tube is higher than that in a normal incidence impedance tube.

Results when a grazing flow of $Ma = 0.117$ passes the liner are depicted in Figs. 11(c) and (d). The acoustic resistance decreases slightly instead of increasing with an increasing SPL_{SP} under the grazing flow, which is opposite to the situation in the absence of grazing flow. As mentioned before, the grazing flow-induced vortex can lead to an increase in the acoustic resistance; however, the presence of a vortex induced by high-intensity sound offsets and reduces the strength of the grazing flow-induced vortex as the SPL_{SP} reaches up to 140 dB. On the other hand, the effect of the SPL is greatly inhibited at relatively high grazing flow Mach numbers as well, i.e., the starting point of the nonlinear range is extended to a much higher SPL. A similar phenomenon was also found in a study by Goldman and Panton.[38] Therefore, the interaction between high SPL and grazing flow effects produces a slight decrease of the acoustic resistance when the SPL_{SP} increases under the grazing flow.

6. Conclusions

In this paper, the straightforward method is applied experimentally in impedance eduction for two pieces of conventional SDOF liners in a flow duct. A numerical sound field is predicted using educed impedance based on an FEM duct propagation model. Subsequently, validation of the SFM accuracy is conducted by means of comparing experimental and numerical sound fields for the first time. Finally, based on comparisons between validated educed impedance data and predictions by three impedance models, the effects of grazing flow and high sound intensity on the impedance behavior of SDOF liners are investigated.

The following conclusions can be drawn:

(1) The educed impedance leads to satisfactory agreements between numerical acoustic attenuation prediction and experimental sound field for both profiles of SPL and phase from 3000 Hz to a frequency as low as 500 Hz

at Mach 0 and 0.146. The fact proves that the straightforward method can provide reliable liner impedance in the absence or presence of grazing flow.

(2) Due to the grazing flow effect, acoustic resistance variation can be divided into two regions, i.e., the sinking region and the linearly increasing region. The starting Mach number and the slope of the increasing region, which are two critical factors to accurately predict the grazing flow acoustic resistance, can be well estimated by the PVM and the KI, respectively. However, the GR fails to consider the sinking region, thus giving only a simple linear relation of resistance starting from Mach zero.

(3) There exists complicated interaction when high sound intensity effect and grazing flow effect are present simultaneously, and the SPL effect can be greatly inhibited when grazing flow is present, while the grazing flow effect can be reduced partly as well at a relatively high SPL_{SP}.

Acknowledgements

The research work was co-supported by the National Natural Science Foundation of China (No. 51576009) and the Projects of International Cooperation and Exchanges National Natural Science Foundation of China (Nos. 11661141020 and 51711530036).

Appendix A.

Table A1 Acoustic pressure A_m and P_h measured by two-microphone pairs at SPL_{SP} = 130 dB on source and exit planes for liner No. 1.

Ma	Point	*f* = 500 Hz		*f* = 1000 Hz		*f* = 1500 Hz		*f* = 2000 Hz		*f* = 2500 Hz		*f* = 3000 Hz	
		A_m/Pa	P_h/rad	A_m/Pa	P_h/rad	A_m/Pa	P_h/rad	A_m/Pa	P_h/rad	A_m/Pa	P_h/rad	A_m/Pa	P_h/rad
0	J_1^S	69.70	0	61.11	0	60.28	0	66.80	0	65.59	0	59.79	0
	J_2^S	65.90	−0.206	56.29	−0.519	73.88	−0.837	78.33	−0.756	47.18	−1.026	63.41	−1.268
	J_1^E	58.63	−1.021	53.18	−2.113	20.24	0.374	6.882	0.602	43.15	2.802	48.05	1.601
	J_2^E	63.55	−1.253	47.68	−2.580	22.59	−0.124	5.847	0.095	22.77	1.547	50.52	−0.205
0.029	J_1^S	66.80	0	57.88	0	57.10	0	56.86	0	69.42	0	58.99	0
	J_2^S	63.22	−0.198	53.37	−0.501	70.27	−0.801	67.74	−0.703	48.74	−0.987	62.66	−1.215
	J_1^E	56.30	−0.785	51.22	−1.575	24.95	1.400	5.883	1.582	46.74	−2.537	47.77	2.741
	J_2^E	61.12	−1.007	45.77	−2.030	27.71	0.929	4.885	1.125	23.78	2.496	50.95	0.956
0.059	J_1^S	68.18	0	63.73	0	66.50	0	55.95	0	67.00	0	59.79	0
	J_2^S	65.19	−0.197	57.41	−0.475	78.76	−0.846	65.02	−0.635	46.12	−0.962	65.81	−1.185
	J_1^E	56.27	−0.558	51.37	−1.069	32.06	2.894	2.376	−2.759	47.08	−1.499	51.22	−2.428
	J_2^E	61.42	−0.781	46.30	−1.498	35.83	2.427	2.006	3.115	23.68	−2.662	53.23	2.080
0.087	J_1^S	69.24	0	58.90	0	64.87	0	58.30	0	67.82	0	60.32	0
	J_2^S	66.52	−0.190	52.13	−0.462	75.77	−0.848	65.83	−0.580	50.54	−0.980	66.35	−1.217
	J_1^E	56.21	−0.340	43.56	−0.588	23.98	−1.967	0.122	−2.626	28.85	−0.307	48.64	−1.249
	J_2^E	61.77	−0.557	39.52	−0.999	26.97	−2.433	0.041	−0.683	14.82	−1.305	45.93	−2.950
0.117	J_1^S	61.16	0	63.02	0	66.62	0	57.82	0	65.50	0	60.93	0
	J_2^S	59.60	−0.179	55.64	−0.431	74.29	−0.857	64.58	−0.671	50.32	−0.952	67.11	−1.300
	J_1^E	48.86	−0.135	44.46	−0.161	20.31	−0.915	0.014	1.167	12.84	0.218	38.92	−0.328
	J_2^E	53.89	−0.346	40.91	−0.535	23.60	−1.424	0.034	−2.808	7.153	−0.550	31.80	−1.928
0.146	J_1^S	67.72	0	68.17	0	60.33	0	62.78	0	64.35	0	69.49	0
	J_2^S	66.48	−0.181	59.86	−0.403	66.36	−0.843	67.32	−0.633	50.16	−0.956	71.36	−1.304
	J_1^E	52.63	0.114	46.59	0.356	18.12	0.128	0.959	0.657	6.445	0.597	32.94	0.615
	J_2^E	58.52	−0.090	43.19	0.008	21.73	−0.403	0.997	0.260	3.938	−0.087	24.53	−0.857
0.175	J_1^S	60.51	0	59.25	0	61.10	0	59.98	0	60.44	0	67.38	0
	J_2^S	60.21	−0.173	52.12	−0.382	65.15	−0.817	65.33	−0.654	47.64	−0.930	64.67	−1.285
	J_1^E	46.30	0.307	39.71	0.755	18.42	0.916	1.860	1.797	3.899	0.644	25.83	1.291
	J_2^E	51.01	0.101	37.00	0.435	22.62	0.352	2.267	1.443	2.807	0.081	17.22	0.011
0.220	J_1^S	59.49	0	61.57	0	61.93	0	58.22	0	62.65	0	58.45	0
	J_2^S	60.90	−0.161	54.69	−0.341	61.42	−0.803	66.36	−0.666	53.11	−0.878	54.72	−1.187
	J_1^E	42.05	0.606	39.18	1.339	19.14	2.110	4.911	−2.943	3.115	0.246	16.34	2.203
	J_2^E	46.84	0.397	38.11	1.070	23.09	1.401	7.493	2.825	3.805	−0.268	11.36	1.323

References

1. Lu YD, Wang QH, Hu ZA, Cui JY. Optimization of acoustic impedance, geometric structure and operating condition of liners mounted in engine duct. *Chin J Aeronaut* 1996;**9**(3):193–203.
2. Watson WR. A method for determining acoustic-liner admit-tance in ducts with sheared flow in two-cross-sectional direc-tions. Washington, D.C.: NASA; 1985. Report No.: NASA-TP- 601 2518.
3. Watson WR. A new method for determining acoustic-liner admittance in a rectangular duct with grazing flow from experi-mental data. Washington, D.C.: NASA; 1984. Report No.: NASA-TP-2310.
4. Watson WR, Jones MG. Impedance eduction in ducts with higher-order modes and flow. Reston(VA): AIAA; 2009. Report No.: AIAA-2009-3236.
5. Watson WR, Jones MG. Validation of a new procedure for impedance eduction in flow. Reston(VA): AIAA; 2010. Report No.: AIAA-2010-3764.
6. Jing XD, Peng S, Sun XF. A straightforward method for wall impedance eduction in a flow duct. *J Acoust Soc Am* 2008;**124**(1):227–34.
7. Jing XD, Peng S, Wang LX, Sun XF. Investigation of straight-forward impedance eduction in the presence of shear flow. *J Sound Vib* 2015;**335**:89–104.
8. Watson WR, Jones MG, June JC. Single mode theory for impedance eduction in large-scale ducts with grazing flow. Reston(VA): AIAA; 2014, Report No.: AIAA-2014-3351.
9. Zhou L, Boden H. Effect of viscosity on impedance eduction and validation. Reston(VA): AIAA; 2015, Report No.: AIAA-2015-2227.
10. Watson WR, Jones MG, Parrott TL. Validation of an impedance eduction method in flow. *AIAA J* 1998;**37**(7):818–24.
11. Watson WR, Jones MG. Comparison of a convected Helmholtz and Euler model for impedance eduction in flow. Reston (VA): AIAA; 2006. Report No.: AIAA-2006-2643.
12. Watson WR, Jones MG, Gerhold CH. Implementation and validation of an impedance eduction technique. Reston (VA): AIAA; 2011. Report No.: AIAA-2011-2867.
13. Naishadham K, Lin XP. Application of spectral domain Prony's method to the FDTD analysis of planar microstrip circuits. *IEEE T Microw Theory* 1994;**42**(12):2391–8.
14. Wisse CJ, Smeulders DM, Van Dongen ME, Chao G. Guided wave modes in porous cylinders: experimental results. *J Acoust Soc Am* 2002;**112**(3):890–5.
15. Watson WR, Carpenter MH, Jones MG. Performance of Kumaresan and Tufts algorithm in liner impedance eduction with flow. *AIAA J* 2015;**53**(4):1091–102.
16. Watson WR, Jones MG, Parrott TL. Investigation of an anomaly observed in impedance eduction techniques. Reston (VA): AIAA; 2008. Report No.: AIAA-2008-3013.
17. WatsonWR, Jones MG. A comparative study of four impedance eduction methodologies using several test liners. Reston (VA): AIAA; 2013. Report No.: AIAA-2013-2274.
18. Watson WR, Jones MG, Tanner SE, Parrott TL. Validation of a numerical method for extracting liner impedance. *AIAA J* 1997;**34**(3):548–54.
19. Kooi JW, Sarin SL, Fokker BV. An experimental study of the acoustic impedance of Helmholtz resonator arrays under a turbulent boundary layer. Reston(VA): AIAA; 1981. Report 652 No.: AIAA 81-1998.
20. Jing XD, Sun XF, Wu JS, Meng K. Effect of grazing flow on the acoustic impedance of an orifice. *AIAA J* 2001;**39**(8):1478–84.
21. Yu J, RuizM, Kwan HW. Validation of Goodrich perforate liner 656 impedance model using NASA Langley test data. Reston 657 (VA): AIAA; 2008, Report No.: AIAA-2008-2930.
22. Myers MK. On the acoustic boundary condition in the presence of flow. *J Sound Vib* 1980;**71**(3):429–34.
23. Eversman W. The boundary condition at an impedance wall in a non-uniform duct with potential mean flow. *J Sound Vib* 2001;**246**(1):63–9.
24. Munjal ML, Doige AG. The two-microphone method incorpo-rating the effects of mean flow and acoustic damping. *J Sound Vib* 1990;**137**(1):135–8.
25. Acoustics-determination of sound absorption coefficient and impedance in impedance tubes—Part 1: Method using standing wave ratio. London: International Organization for Standardiza-tion; 1996. Standard No.: ISO 10534-1.
26. Acoustics-determination of sound absorption coefficient and impedance in impedance tubes—Part 2: Transfer function method. London: International Organization for Standardization; 1998. Standard No.: ISO 10534-2.
27. Jones MG, Watson WR, Tracy MB, Parrott TL. Comparison of two waveguide methods for educing liner impedance in grazing flow. *AIAA J* 2004;**42**(2):232–40.
28. Jones MG, Watson WR, Parrott TL. Benchmark data for evaluation of aeroacoustic propagation codes with grazing flow. Reston(VA): AIAA; 2005. Report No.: AIAA-2005-2853.
29. Li XD, Richter C, Thiele F. Time-domain impedance boundary conditions for surfaces with subsonic mean flows. *J Acoust Soc Am* 2006;**119**(5):2665–76.
30. Richter C, Thiele FH, Li XD, Zhuang M. Comparison of time-domain impedance boundary conditions for lined duct flows. *AIAA J* 2007;**45**(6):1333–45.
31. Reymen Y, Baelmans M, Desmet W. Time-domain impedance formulation suited for broadband simulations. Reston (VA): AIAA; 2007. Report No.: AIAA-2007-3517.
32. Burak MO, Billson M, Eriksson LE, Baralon S. Validation of a time- and frequency-domain grazing flow acoustic liner model. *AIAA J* 2009;**47**(8):1841–8.
33. Guo Y, Allam S, Abom M. Micro-perforated plates for vehicle applications. *37th INTER-NOISE and NOISE-CON congress 694 and conference proceedings*; 2008 Oct 26–29; Shanghai, China. Stockholm: KTH; 2008.
34. Guess AW. Calculation of perforated plate liner parameters from specified acoustic resistance and reactance. *J Sound Vib* 1975;**40**(1):119–37.
35. Lewis GD, Garrison GD. The role of acoustic absorbers in preventing combustion instability. Reston(VA): AIAA; 1971. Report No.: AIAA-71-699.
36. Cummings A. The effects of grazing turbulent pipe-flow on the impedance of an orifice. *Acta Acust United Ac* 1986;**61**(4):233–42.
37. Kurbatskii KA, Tam CKW. Microfluid dynamics and acoustics of resonant liners. *AIAA J* 2000;**38**(8):1331–9.
38. Goldman AL, Panton RL. Measurement of the acoustic impe-dance of an orifice under a turbulent boundary layer. *J Acoust Soc Am* 1976;**60**(6):1397–404.